Failure analysis of two aluminium alloy sonotrodes for ultrasonic plastic welding

Michele Carboni *

Department of Mechanical Engineering, Politecnico di Milano, Via La Masa 1, 20156 Milano, Italy

Article history:
Received 18 April 2012
Received in revised form 8 March 2013
Accepted 24 May 2013
Available online 5 June 2013

1. Introduction

Ultrasonic welding (USW) [1] is an industrial technology that employs ultrasonic vibrations, applied locally to a number of parts, in order to create a solid-state joint. USW is widely used for thermoplastics [1], but is also applied to light alloys in some specific fields [2,3] and can be applied to dissimilar materials or complex geometrical parts.

Ultrasonic welding of thermoplastics (USPW) is typically used to join the small parts that are used in the production of items such as cell phones, consumer electronics, disposable medical tools, toys, packaging, etcetera, but it can also be applied to parts as large as an automotive instrument cluster. The welded joint is realised [4] in a very short time through the local melting of the parts due to the absorption of vibration energy (frictional heat) that is generated by a dedicated manufacturing system. Fig. 1a shows the schematic of a typical welder. The parts to be welded are placed [5] between a holding plate (anvil) and an ultrasonic stack which is composed by a converter (a piezoelectric transducer which converts electrical signals into mechanical vibrations), a booster (typically used to increase the amplitude of the mechanical vibrations) and a sonotrode (the part of the manufacturing system that is actually in contact with the parts to be welded). It is worth noting that a clamping force is applied to the parts before beginning the welding process and that the vibration is perpendicular to the parts to be welded (Fig. 1a). Depending on the plastic material to be welded [1], the typical vibration amplitude is 20 μm beginning at the piezoelectric transducer and then reaches an amplitude of 30–60 μm once it arrives to the welding surface of the sonotrode. The ultrasonic stack is designed to work in a resonant condition at the frequency of the electrical signal applied to the piezoelectric transducer; typically ranging from 15 kHz to 70 kHz, where the most usual values are 20 kHz or 35 kHz in order to achieve a suitable vibration amplitude at the welding surface.

A sonotrode is produced using metallic materials [5]; with around 85% of sonotrodes produced in aluminium alloys, 10% in titanium alloys (this percentage is continually increasing) and 5% in steel. The optimised design [1] of a sonotrode, both in terms of its shape (round, rectangular, etc.) and its so-called "features" (through-passing holes, changes of dimensions, etc.), is based on the quantity of vibration energy (which is directly related to the working frequency, the vibration amplitude and the material to be welded) needed for a proper weld and on the shape and dimensions of the weld to be achieved. Therefore, the sonotrode must be optimally designed for each application, while the other parts of the welder are kept the same. Fig. 1b demonstrates just how varied the morphology of sonotrodes can be. It must be acknowledged that, today, the design of sonotrodes is still based on rather old guidelines [1] and on the direct experience of producers where many procedures are often proprietary and not publicly disclosed. In addition, the design usually implements analytical, numerical or experimental approaches in order to characterise the natural frequencies to be coupled with the working frequency, but without taking into consideration an assessment of the structural integrity. This is most likely due to the fact that the dynamical design is usually enough to prevent structural failures. This hypothesis is

* Tel.: +39 02 23998253; fax: +39 02 23998202.
E-mail address: michele.carboni@polimi.it

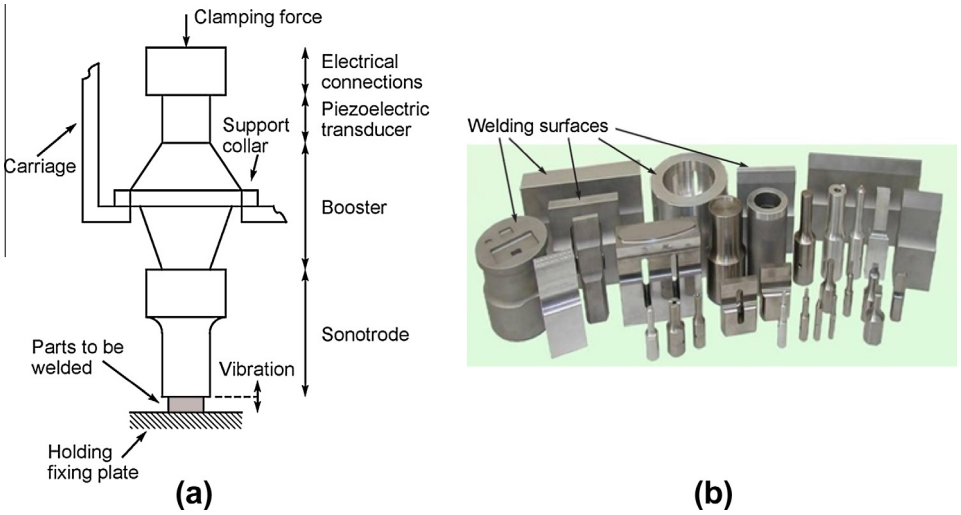

Fig. 1. Ultrasonic welding of thermoplastic materials: (a) scheme of a typical welder; and (b) examples of different geometries of sonotrodes.

supported by the fact that very few service failures actually happen. A direct consequence of this is that no relevant scientific studies on the structural behaviour of sonotrodes are available and their service stresses are not yet fully known or understood.

A well designed sonotrode works on average for a ten-year period and carries out a number of expected (stress) working cycles to the order of 10^{12} if the working frequency is 20 kHz. The following research is focused on the analysing the premature failure of two sonotrodes made of AA7075-T6 and used for USPW at a working frequency of 20 kHz. These premature failures occurred at about 5×10^9 working cycles, corresponding to a few working weeks; a value that is significantly lower than the expected one of ten years. It is worth mentioning that identical sonotrodes (made from other batches of AA7075-T6, having exactly the same geometries and applied to the same welding procedure) did not suffer any failure for a much higher number of service cycles. Since the order of magnitude of the number of cycles to failure is significantly higher than the one typically considered in traditional high cycle fatigue, the present cases can be identified by very high cycle fatigue (VHCF) phenomena [6]. The relationship between unexpected defects and the very high cycle fatigue strength for the two sonotrodes was detected after carrying out non-destructive testing (NDT) analysis in order to understand the reasons of the premature failures as well as observations made possible through the use of a scan-electron microscope (SEM), metallurgical analyses and dynamic finite elements (FEM) analyses.

2. Experimental failure analysis of the sonotrodes

2.1. Non-destructive inspection

The premature failures of the considered sonotrodes (Fig. 2a and b) were discovered during service and as a result of poor quality in the welds. In particular, the quality of an ultrasonic weld of thermoplastics is usually defined in terms of its effective realisation and its static strength and depends on ([4,5]) the uniformity of the heat generated by the vibrating welding surface of the sonotrode and applied to the parts to be welded. This uniformity in heat is strictly related to the displacement field of the welding surface, which should be as uniform as possible. If cracks initiate somewhere in an optimised sonotrode, its stiffness will change, thus, causing a modification in the dynamical behaviour of the whole welder and the uniformity of the displacement field cannot be guaranteed any more.

These observations suggested the need to investigate the possible initiation and propagation of fatigue cracks in the sonotrodes. Colour contrast liquid penetrants were applied since a visual inspection could not reveal any particular geometrical or material inhomogeneity. The results of this inspection revealed (Fig. 3a and b) the presence of numerous cracks that were characterised by visible dimensions of tens of millimetres and found at different stress concentration regions. It is reasonable to assume that the cracks initiated at stress concentrations where service stresses were higher. However, in this case, such concentrations cannot be assumed as the only reason when considering that numerous other sonotrodes made of AA7075-T6, having exactly the same geometries and applied to the same welding procedure did not suffer any failure and are still in service after some years. The two sonotrodes analysed here failed after only a few weeks, suggesting that other factors might have played a role in a synergic combination with geometrical stress concentrations. Theses possible factors were, consequently, investigated.

2.2. Fractography of fracture surfaces

The fracture surfaces of all the cracks were observed using a SEM in order to further understand the origins of the premature failures. The two sonotrodes were properly cut and the crack surfaces separated. Fig. 4a and b document the cracks found in the rectangular and circular sonotrode respectively. It must be added that all the cracks initiated at the stress concentrations located at the opposite side of the welding surface; i.e. at the side where the sonotrode is connected to the booster.

First, analyses employing secondary electrons [7] were made in order to observe the topography of fracture surfaces and to individuate the initiation sites of the fatigue cracks. These analyses allowed for the categorisation of all of the initiation sites into two different types.

The first type was observed in seven of the ten fracture surfaces and occurred in the interior of the material (as is expected in very high cycle fatigue [8,9]), close to stress concentrations and at a distance equal to about 1 mm from the surface. See Fig. 4a and b for an indication of the locations in the two sonotrodes. Fig. 5a shows a relevant example from the prismatic sonotrode: crack initiation occurred in a particular region where no exogenous inclusions or defects could be found (Fig. 5b). This could have been expected since it is known [10] that AA7075 usually shows porosities and oxides as initiation regions, at least, in high cycle fatigue. From this

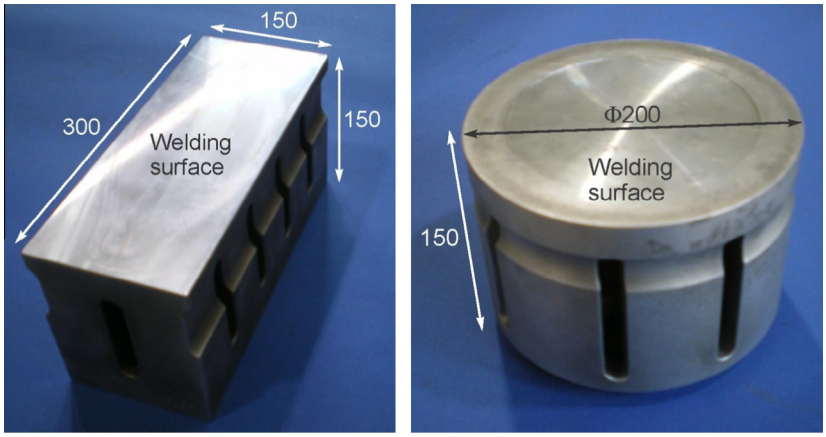

Fig. 2. Prematurely failed sonotrodes (dimensions in (mm)).

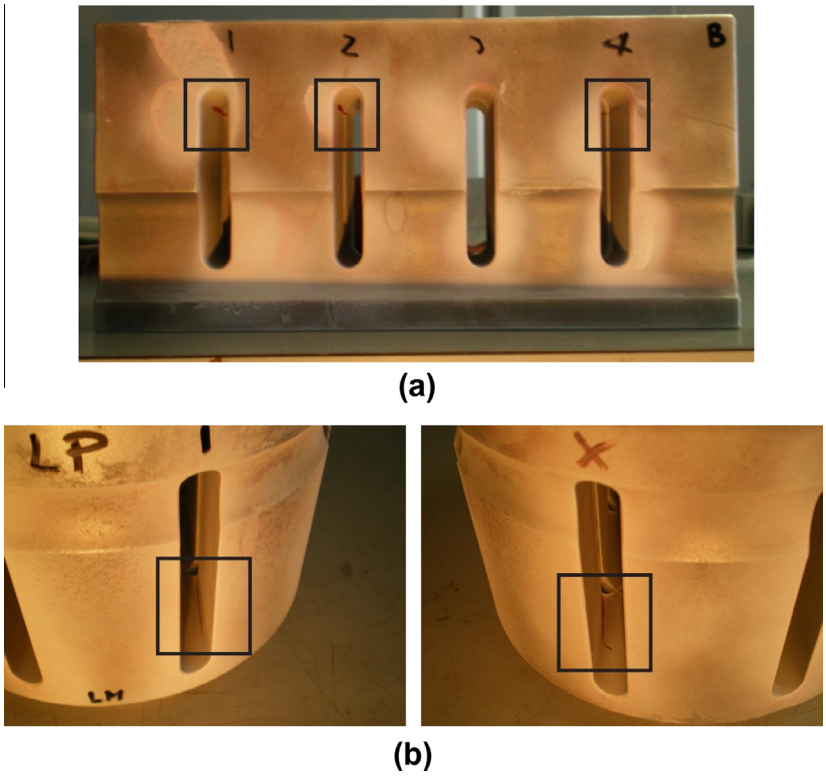

Fig. 3. Colour contrast liquid penetrants applied to reveal fatigue cracks.

region, two different types of radial propagation were observed: a transgranular, brittle one characterised by the typical facets of cleavage [11] and propagating towards the external border and a ductile one characterised by dimples [11] and propagating towards the interior of the sonotrode.

The second type of initiation site, represented in the remaining three fracture surfaces, occurred just below the surface (see Fig. 4a and b for an indication of the locations in the sonotrodes). Fig. 6a and b show an example of this in the circular sonotrode. In this case, as well, two different propagation regions were observed: the first one located around the initiation site at the border of the sonotrode and characterised by a transgranular, brittle behaviour and a particular inclination with respect to the vibration direction, while the second one is characterised by a ductile propagation towards the interior of the sonotrode and is perpendicular to the vibration direction.

In order to show the possible presence of local or diffused material inhomogeneities, all the initiation sites were observed through the means of back-scattered electrons using the quarter back-scattered diffraction (QBSD) technique [7] available on the SEM. Figs. 5c and 6c show the results for the examples already described above. In particular, Fig. 5c shows the initiation site for the first type of failure, which seems to be quite corrugated and characterised by a significantly different grade of the grey scale, thus, suggesting an atomic number of the local material chemical composition different from that of the surrounding one. This is reminiscent of what Murakami et al. [12] found during very high cycle fatigue testing of steels and termed "optically dark area"

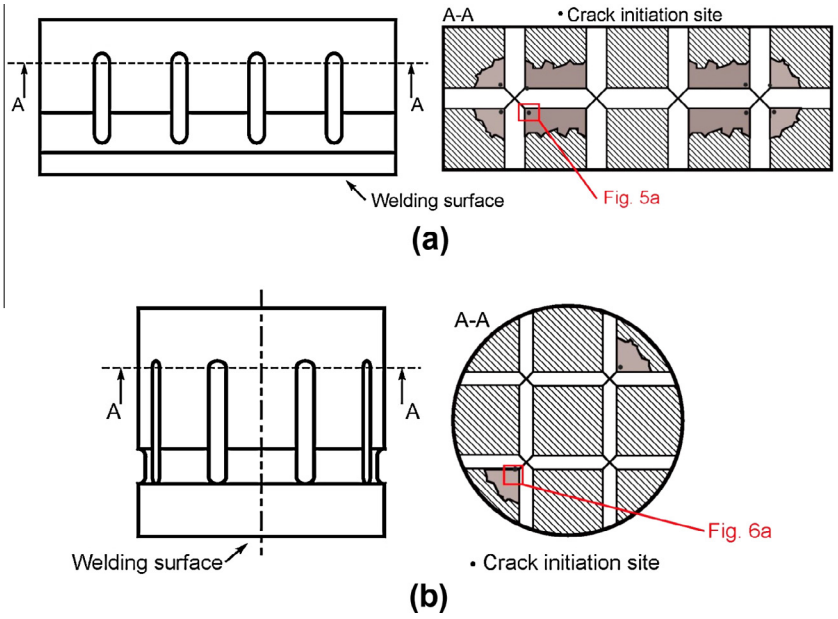

Fig. 4. Schemes of the found fatigue cracks: (a) rectangular sonotrode; (b) circular sonotrode.

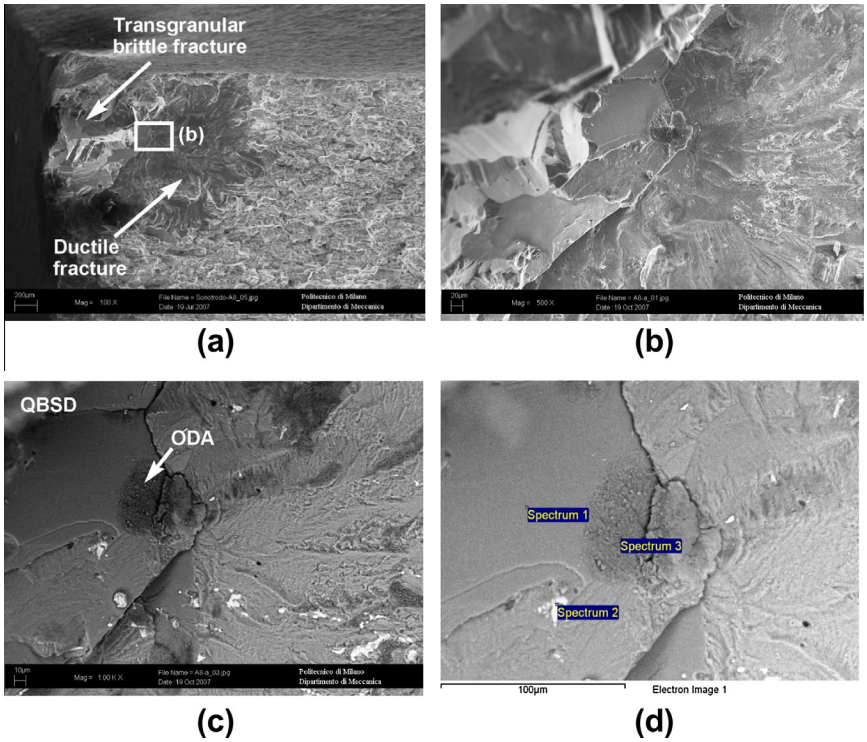

Fig. 5. An example of SEM investigation, carried out on a fracture surface coming from the prismatic sonotrode, of the first type of failure: (a) region of crack initiation; (b) detail of the initiation site; (c) QBSD analysis of the initiation site; and (d) EDS analysis of the initiation site.

(ODA). However, there is one fundamental difference: an inclusion is needed to trap hydrogen in steels, while for AA7075-T6, as stated above, no exogenous inclusions or defects could be found. Nevertheless, the dark areas observed at the initiation sites of this first kind of failure will still be termed "ODA" because an optically dark area was observed. To better understand these initial observations, an energy-dispersive X-ray spectroscopy (EDS) technique [7] was employed, using the SEM, in order to chemically characterise the sample. Three different punctual locations of the fracture surface were analysed (Fig. 5d). Table 1 shows the obtained results compared to the expected chemical composition defined by the relevant standards [13] for AA7075. It must be stated that EDS is a semi-quantitative [14] approach and, therefore, the reported quantities have to be evaluated considering the limitations of the method. Moreover, the application of punctual analyses could show chemical compositions related to local features. For these reasons, more refined metallurgical analyses of the material will be described in Section 2.3. The first point of measurement (Spectrum

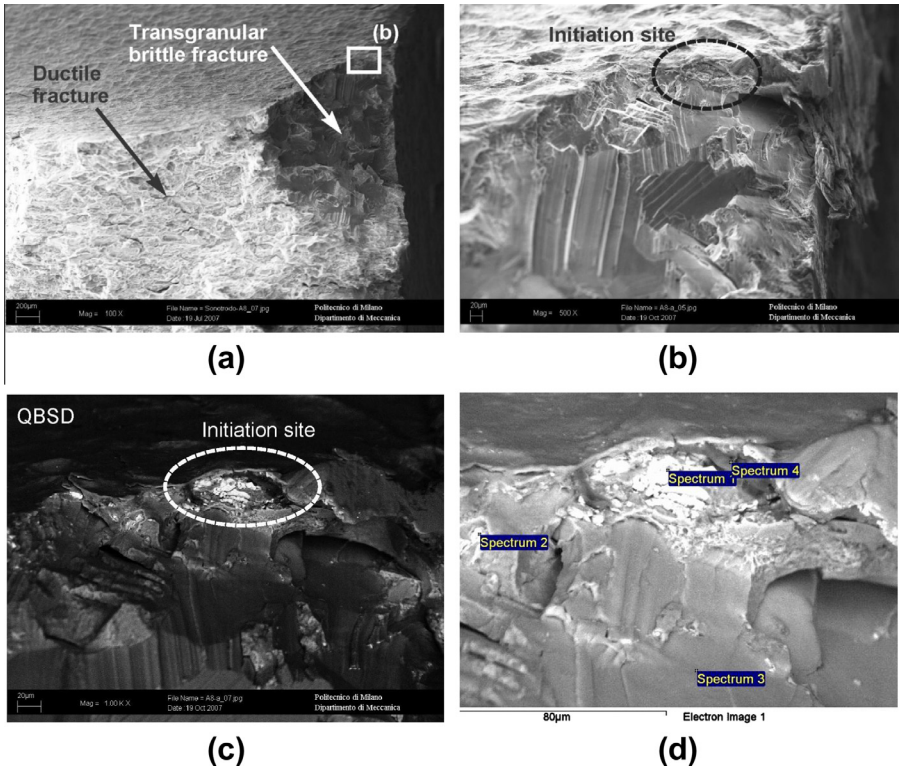

Fig. 6. An example of SEM investigation, carried out on a fracture surface coming from the cylindrical sonotrode, of the second type of failure: (a) region of crack initiation; (b) detail of the initiation site; (c) QBSD analysis of the initiation site; and (d) EDS analysis of the initiation site.

Table 1
EDS chemical analysis of the initiation region of the first type of failure (in weight %).

	O	Mg	Al	Mn	Fe	Cu
Expected chemical composition [13]		2.1–2.9	Bal.	⩽0.3	⩽0.5	1.2–2.0
Spectrum 1		1.41	57.63			40.95
Spectrum 2		0.56	60.23	4.54	7.58	27.10
Spectrum 3	40.2	1.55	51.54			6.72

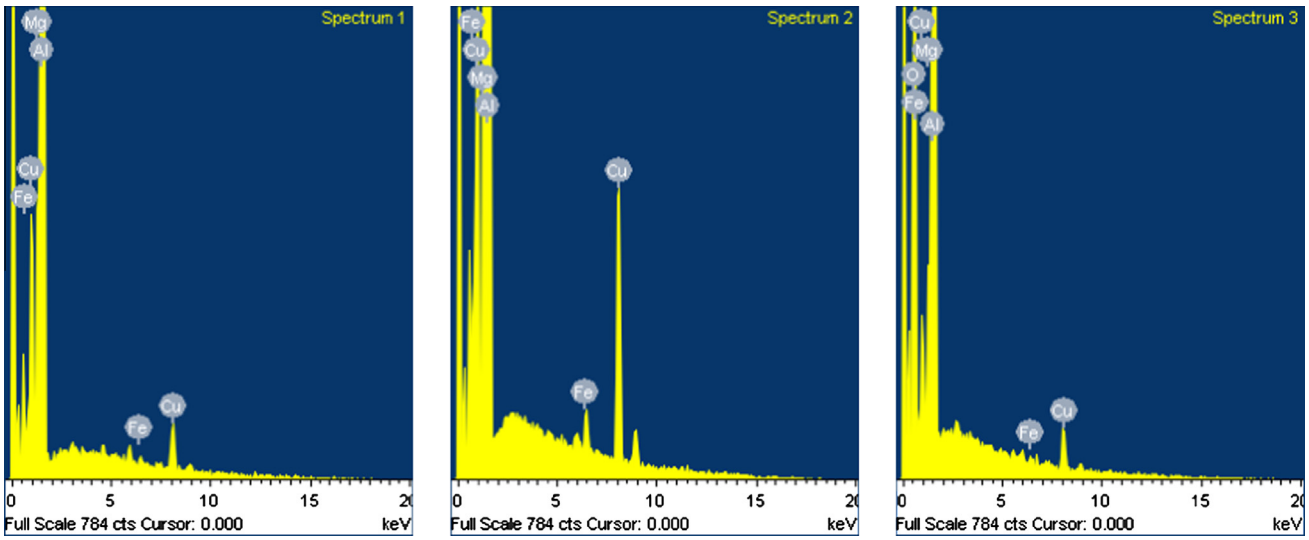

Fig. 7. Punctual EDS spectra of the spots shown in Fig. 5d (rectangular sonotrode).

1, Fig. 7) was chosen due to the absence of any relevant indication as a reference of the material; however, a lower percentage of magnesium was found, with respect to the expected percentage, together with an extremely high percentage of copper. The second point (Spectrum 2, Fig. 7) was measured with correspondence to a punctual indication that was characterised by a low percentage

of magnesium and high percentages of copper, manganese and iron. Finally, the third point (Spectrum 3, Fig. 7) was measured inside the initiation ODA region where high concentrations of oxygen and copper were observed together with a low percentage of magnesium. This is an important observation because it represents another fundamental difference with respect to VHCF in steels: it seems that, at least for AA7075, oxygen plays a key role instead of hydrogen. The reason is unclear because oxygen's molecular size is bigger than hydrogen's one and, consequently, its diffusion into metals should be more difficult. This point will be further analysed in Section 2.3. Each of the fracture surfaces related to the first type of failure exhibited the same features described in Fig. 5.

The same QBSD and EDS analyses were carried out at all of the initiation sites of the second type of failure. Fig. 6c shows the QBSD analysis and demonstrates the presence of an aggregate found at the initiation site that is characterised by a different atomic number with respect to the surrounding material. It is worth noting that no ODAs were observed at subsurface initiation sites for this second type of failure. Fig. 6d and Table 2 respectively show the punctual locations of the four EDS measurements carried out and the obtained results. The first point of measurement (Spectrum 1, Fig. 8) corresponds to the aggregate at the base of the failure and showed large percentages of copper, iron and manganese together with a lower-than-expected percentage of magnesium. The second measurement point (Spectrum 2, Fig. 8) represented another dishomogeneous region that is close to the initiation site and, once again, characterised by high percentages of copper, iron and manganese and a low percentage of magnesium. The third and fourth measurement points (Spectrum 3 and Spectrum 4, Fig. 8) were representative of the base material, but showed high percentages of copper, iron and manganese, a low percentage of magnesium and the presence of silicon. Each fracture surface of the second type of failure showed similar features to those described in Fig. 6.

Proper metallurgical techniques were then employed to further analyse the material in order to better understand the strange chemical composition of the material at the initiation sites.

2.3. Metallurgical analyses of the considered AA7075-T6

The quantitative chemical composition of 7075-T6 alloy was derived using mass spectrometry [14] applied by a quantometer. In particular, five different areas were measured: three from the rectangular sonotrode (two close to one of the failure regions and one far from any of them) and two from the circular one (one close to one of the failure regions and one far from any of them). Table 3 shows the results compared to the expected chemical composition [13]. It seems that the 7075 alloy is quite repeatable at different locations of the sonotrodes and very well aligned with the typical 7075 alloy; thus, suggesting the absence of problems related to its chemical composition at the base of the observed failures, but also revealing a possible contradiction with the results obtained by the EDS analyses carried out on fracture surfaces in Section 2.2.

The same five regions analysed by the quantometer were then observed through an optical microscope (after proper polishing) in order to verify the micro-structure of the material. All of the five areas (i.e. both close to and far from initiation regions) showed comparable micro-structural patterns denoting the generalised condition of the material which is exemplified in Fig. 9. As can be seen, the 7075-T6 aluminium alloy is extremely segregated at grain boundaries and such segregation seems to be uniformly distributed throughout the entire volume of the sonotrodes. The reason for this segregation is beyond the aim of the present research; however, since the chemical composition was found to be correct, it may be hypothesised as having to do with an improper heat treatment. It is also worth noting that such widespread segregation might weaken the strength of the basic matrix of the material (acting as a huge cluster of endogenous defects and helping the development of unexpected fatigue damage) especially in VHCF conditions as described in the following.

Finally, the five regions were analysed using the SEM so as to identify which chemical element or elements segregated at grain boundaries. Fig. 10a and b respectively provide a detailed example of the segregation using secondary electrons and QBSD. Regarding the QBSD analysis, it is worth noting the presence of pores, significantly bigger than the ones in the matrix, that are found within the segregation itself. Table 4 reveals the EDS analysis of the same sample shown in Fig. 10. While the chemical composition of the matrix is compliant with the expected one, at least within the limits of EDS, the segregation is characterised by significant percentages of copper, iron and manganese, as well as oxygen. The former chemical elements composing the segregation (Cu, Fe and Mn) can explain the second type of failure where the subsurface aggregates observed at initiation sites (as the one shown in Fig. 6c) were in fact composed of those elements (see Section 2.2). This suggests that segregated particles of a suitable dimension and located very close to the maximum geometrical stress concentrations could have acted as endogenous defects and might have been able to initiate VHCF cracks. These same elements might also explain the contradiction between the results obtained by EDS in Section 2.2 and the ones obtained by mass spectrometry, as punctual EDS analyses likely measured the chemical content of local segregations.

Particular attention must be given to the presence of oxygen in both the segregation and the matrix, even if the percentage of oxygen was much smaller in the latter (Table 4). This seems to support the possibility of an active interaction where oxygen is primarily trapped in the segregation but with the slight ability to diffuse into or to interact in some way with the matrix. This could provide the basis for the idea that an ODA mechanism took place in this particular segregated 7075-T6 aluminium alloy. Contrary to what usually occurs in steels, where hydrogen and exogenous inclusions or defects might initiate VHCF failures, here endogenous defects (the segregation) and the oxygen trapped inside them seem to play a fundamental role. This could be quite interesting to investigate in future research, especially when considering that the rationale for an ODA, in this case, cannot be the embrittlement due to hydrogen, but more probably a damage mechanism based on corrosive phenomena (see again the corrugated ODA in Fig. 5c).

One final comment must be made regarding the two observed failure modes: even if they are phenomenologically different, both

Table 2
EDS chemical analysis of the initiation region of the second type of failure (in weight %).

	Mg	Al	Si	Mn	Fe	Cu
Expected chemical composition [13]	2.1–2.9	Bal.		⩽0.3	⩽0.5	1.2–2.0
Spectrum 1	0.72	48.43		1.68	4.36	44.81
Spectrum 2	1.77	87.51		0.85	1.88	7.99
Spectrum 3	1.24	85.73	1.10	0.89	2.07	8.96
Spectrum 4	1.24	85.95	0.82	0.54	1.75	9.69

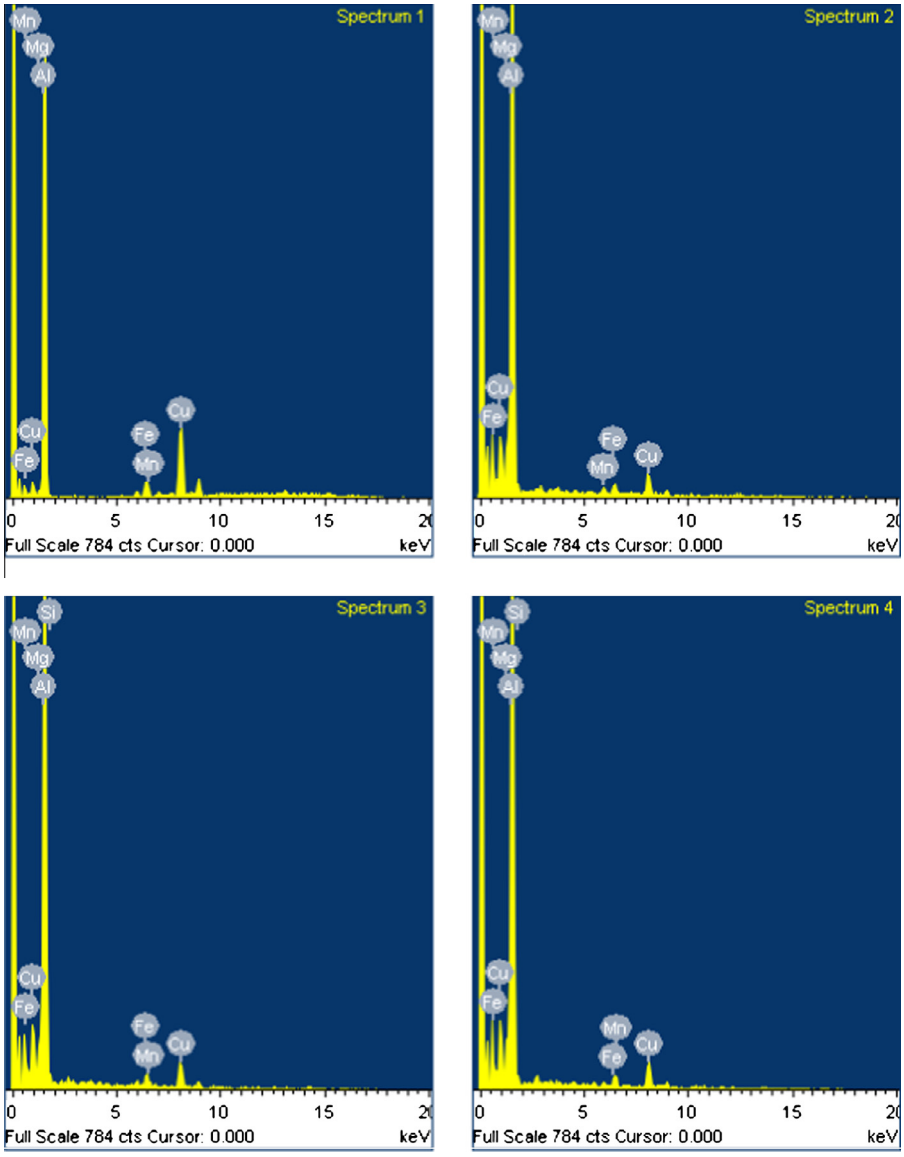

Fig. 8. Punctual EDS spectra of the spots shown in Fig. 6d (circular sonotrode).

Table 3
Mass spectrometry analysis of AA7075-T6 (in weight %).

	Mg	Al	Si	Mn	Fe	Cu	Zn
Expected chemical composition [13]	2.1–2.9	Bal.		⩽0.3	⩽0.5	1.2–2.0	5.1–6.1
Area 1	2.10	90.7	0.0189	0.0278	0.122	1.41	5.29
Area 2	2.16	90.6	0.0117	0.0292	0.128	1.36	5.39
Area 3	2.18	90.6	0.0567	0.0292	0.111	1.34	5.37
Area 4	2.14	90.8	0.0074	0.0289	0.0857	1.28	5.29
Area 5	2.18	90.6	0.0157	0.0293	0.0981	1.39	5.41
Mean value	2.15	90.7	0.0221	0.0289	0.109	1.36	5.35

of them were initiated by the segregation. This suggests competition between the two failure modes that is likely based on the dimension of the subsurface segregated particles located very close to the maximum geometrical stress concentrations. Therefore, for a specific geometrical stress concentration, if the dimension of such a particle was big enough, the crack would initiate at the subsurface. However, if the opposite was true, the ODA mechanism would have the time and the possibility to develop in the interior and make the sonotrode fail regardless.

3. Dynamic finite element analysis of service stresses

As stated in the introduction, sonotrodes, today, are designed only on the basis of their dynamical behaviour. Finite element analyses are regularly applied to optimise the geometry of a sonotrode so as to obtain a natural axial frequency as close as possible to the working frequency provided by the piezoelectric transducer. In general, the adopted FEM models are used (for an example, see [1] and [15,16]) to analyse the free vibration conditions of the

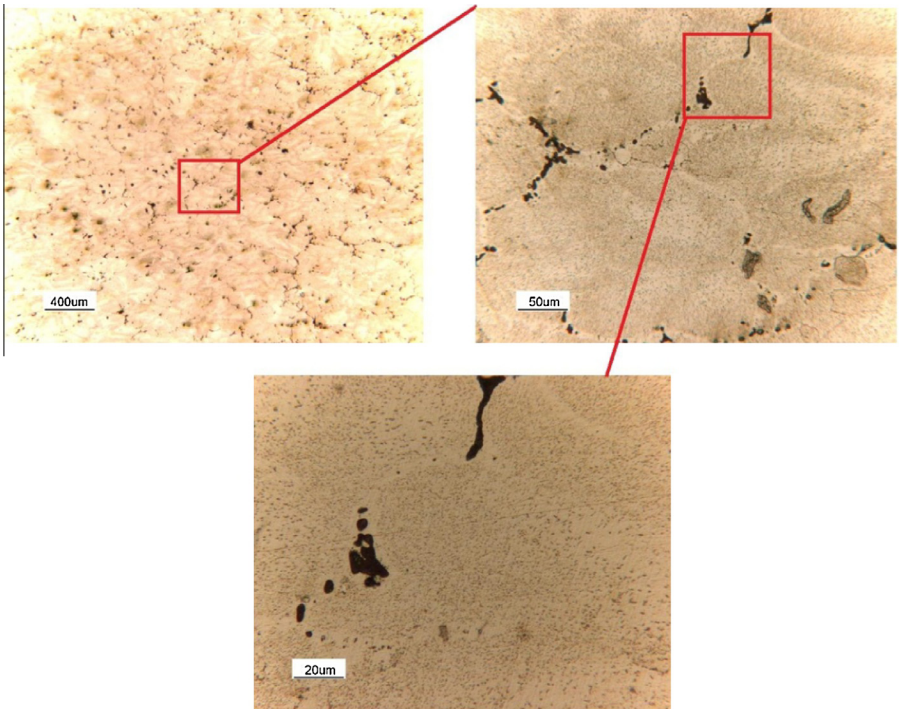

Fig. 9. Micro-structure of the analysed AA7075-T6 observed at the optical microscope.

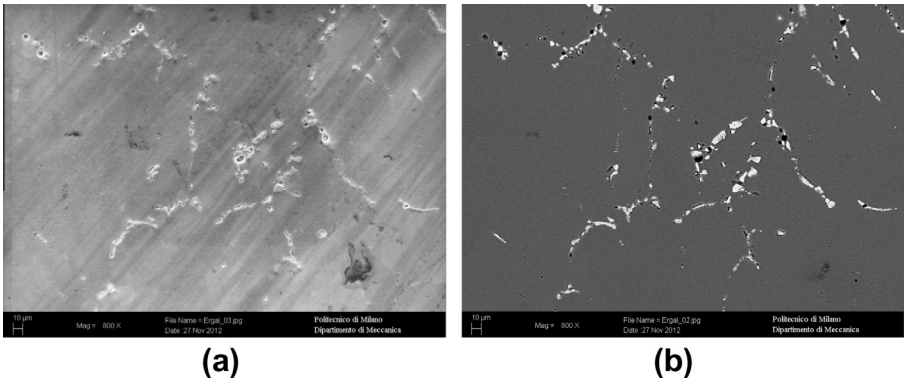

Fig. 10. SEM analysis of segregations at grain boundaries: (a) secondary electrons; and (b) QBSD.

Table 4
EDS chemical analysis of the segregation and the matrix (in weight %).

	Mg	Al	Mn	Fe	Cu	O
Segregation		45.81	4.91	6.67	35.88	6.47
Matrix	1.73	92.06	0.33		4.55	0.94

sonotrode without taking into account any of the other parts of the welder or any boundary condition. With the aim of deriving the service stresses used for the assessment of structural integrity, this approach is too simplistic and so the complete vibrating group (composed by the booster, the sonotrodes, the flanges and all of the relevant connections between parts and the proper boundary conditions) had to be modelled. For what is known at present, a complete FEM analysis of this kind is not available in the existing scientific literature on sonotrodes.

Dynamic FEM analyses were carried out through ABAQUS v. 6.10-1 software [17]. Figs. 11a and 12a show the solid geometries considered during the simulations for the rectangular and the cylindrical sonotrodes, respectively. As can be seen, the geometrical models were properly partitioned for the subsequent application of structural meshes, while only half of the modelled welders are shown in the figures in order to allow for a better description of all the considered parts. Instead, the piezoelectric transducer was modelled by an alternated sinusoidal vibratory displacement imposed on the top surface of the booster and characterised by an amplitude equal to 20 μm and a frequency of 20 kHz because of the fact that its geometrical and material details were not made available due to the proprietary nature of the information. Finally, the influence of the parts to be welded on the vibrating behaviour was modelled by applying a set of springs to all of the nodes of the welding surface with a stiffness equal to 1000 N/mm.

Figs. 11b and 12b show the structural (i.e. mapped) meshes applied to the solid models. Specifically, C3D8 elements (i.e. hexahedral linear elements with eight nodes and complete integration [17]) were used for all of the vibrating group, using an average dimension equal to 5 mm. The properties of the materials used were set (Table 5) in terms of their elastic constants and of their density. Moreover, the structural damping of the vibrating group

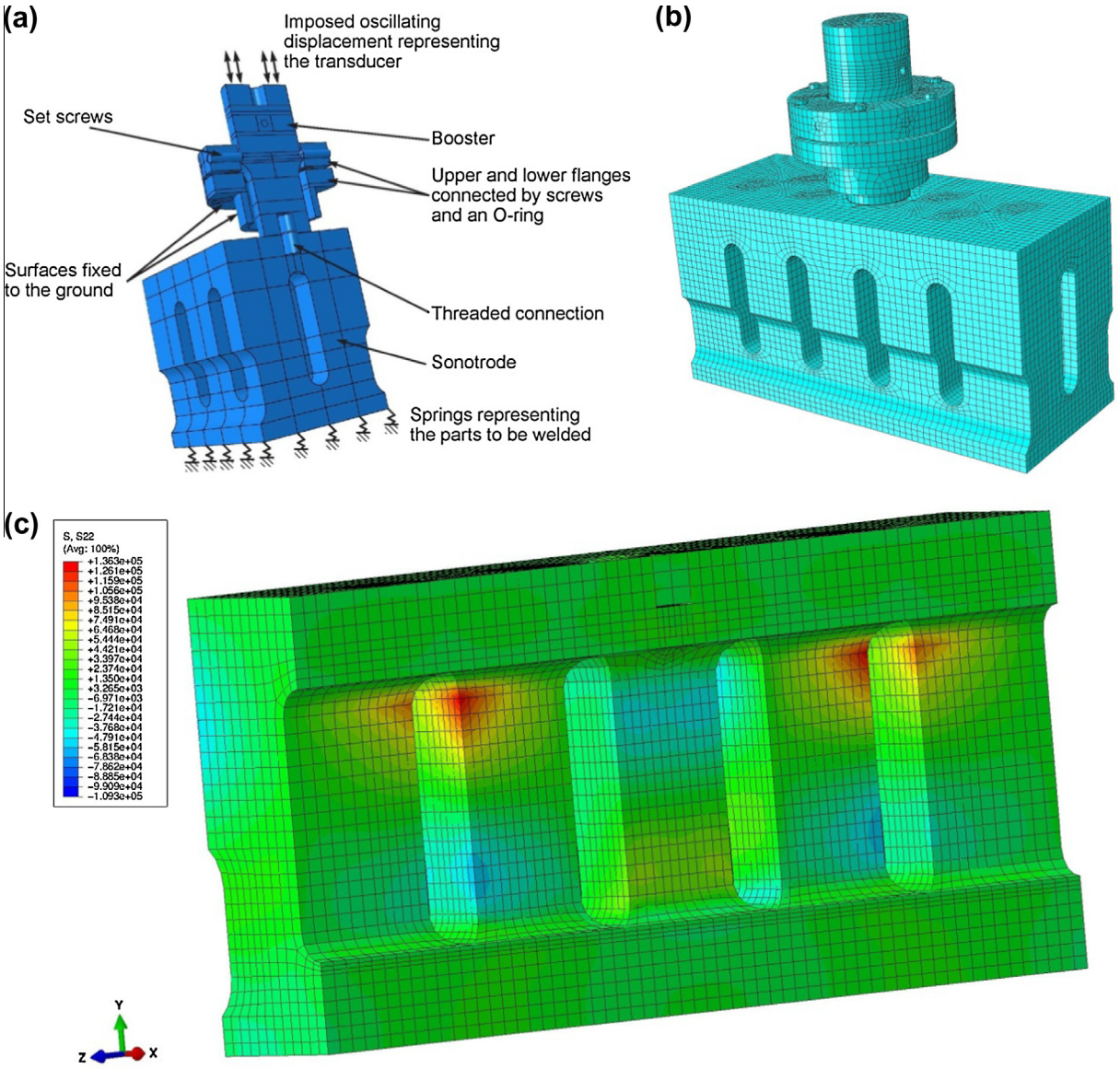

Fig. 11. Dynamic FEM analysis of the rectangular sonotrode: (a) solid model; (b) applied mesh; and (c) stress pattern perpendicular to cracks planes (stress levels in (mN/mm^2)).

was described using Rayleigh's coefficients α and β [17] which are related to the generalised dimensionless damping h by the expression:

$$h = \frac{\alpha}{2\omega} + \frac{\beta\omega}{2} \quad (1)$$

where $\omega = 2\pi f$ and f is equal to 20 kHz for the present case. The α term was assumed to be negligible due to the high ω value, while h was measured (on a welder identical to the considered one [18]) to be equal to 0.0003. The resulting β value is reported in Table 5. Finally, the connections between parts were realised by master-slave "tie" interactions, while the application of the sinusoidal vibration to the top of the booster and the springs to the welding surface was realised using master-slave "coupling" interactions.

First, the natural frequencies of the vibrating group were determined around the nominal working frequency. A range of 19–21 kHz was then spanned during the finite element analyses resulting in an axial vibration mode of 19873 Hz for the vibrating group equipped with the rectangular sonotrode and of 19931 Hz for the circular sonotrode. These values suggested an accurate modelling of the vibrating system. It is worth noting that different natural flexural and torsional vibration modes were also observed, but all of them resulted to be further from the nominal working frequency with respect to the axial ones.

Then, the dynamical behaviour of the vibrating group under the application of the vibratory excitation, for both sonotrodes, was analysed by means of implicit, steady-state, direct, dynamical analyses. The axial displacements at the welding surfaces were equal to 55 μm for the rectangular sonotrode and 39 μm for the circular one. Both values are consistent with those reported in the literature [1]. Figs. 11c and 12c show, as nodal averages extrapolated from the integration points, the stress pattern along the vibration direction, i.e. the one opening the observed cracks by Mode I. As can be seen, the location of the maximum stresses corresponds exactly to the one of service failures and such stress amplitudes resulted to be equal to 136 MPa for the rectangular sonotrode and 96 MPa for the circular one.

4. Influence of defects on fatigue strength

The endurance stress amplitude of AA7075-T6 at $R = -1$ and at 1×10^9 cycles was found in the literature ([19,20]) and is equal to

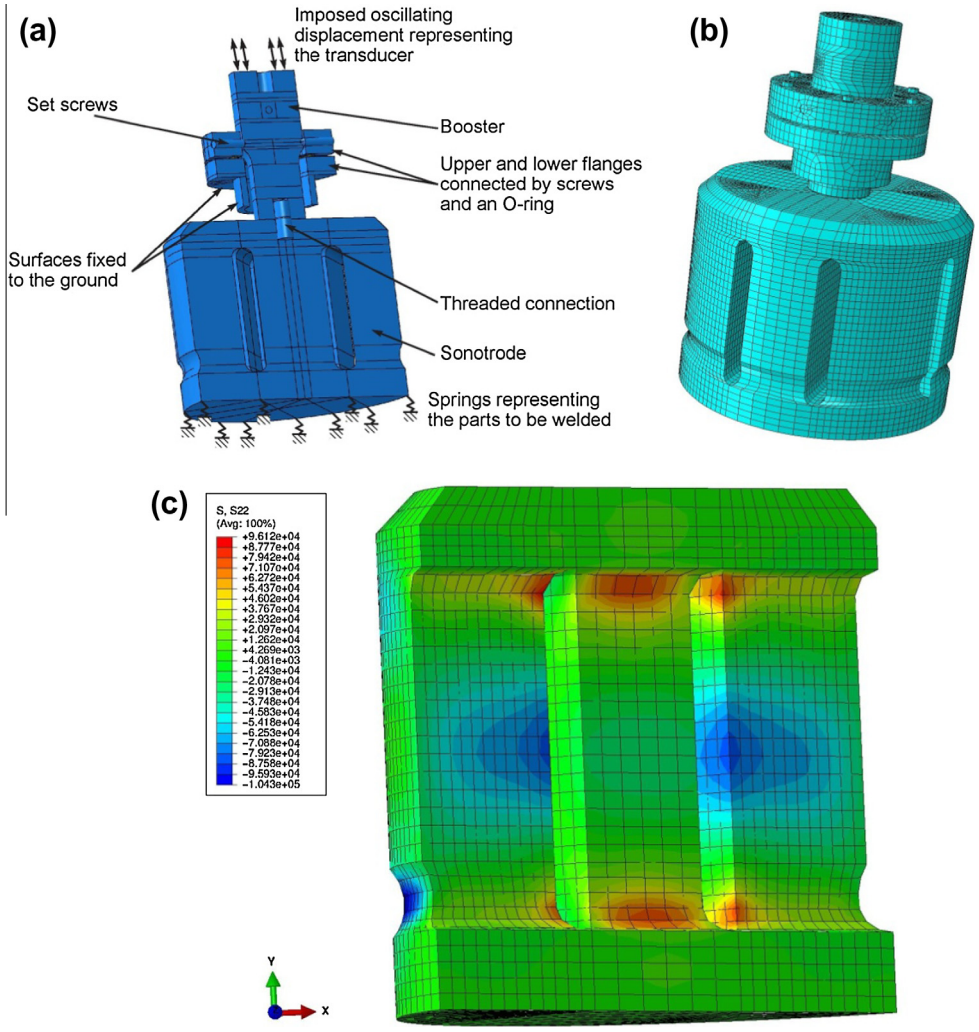

Fig. 12. Dynamic FEM analysis of the circular sonotrode: (a) solid model; (b) applied mesh; and (c) stress pattern perpendicular to cracks planes (stress levels in (mN/mm^2)).

Table 5
Properties of the materials involved in finite element analyses.

Material	Component	Mass density (Kg/dm^3)	Young's modulus (MPa)	Poisson's modulus	Damping coefficient β
AA7075-T6	Sonotrodes and booster	2.8	72000	0.3	4.8×10^{-9}
AISI304 steel	Screws and set screws	7.9	200000	0.3	4.8×10^{-9}
S235 steel	Flanges	7.87	190000	0.3	4.8×10^{-9}

190 MPa. Considering the working stresses obtained from dynamical FEM analyses, this suggests an important and serious detrimental effect due to the initiation defects described in Section 2 on the fatigue strength of AA7075-T6. This effect was then quantified adopting the approach proposed by Murakami [21], where the fatigue endurance strength σ_w is related to the material and to the dimension of a defect and is described by the following equations:

$$\text{Defect in touch with surface}: \ \Delta\sigma_w = \frac{1.41 \cdot (H_v + 120)}{(\sqrt{\text{area}})^{1/6}} \qquad (2)$$

$$\text{Internal defect}: \ \Delta\sigma_w = \frac{1.56 \cdot (H_v + 120)}{(\sqrt{\text{area}})^{1/6}} \qquad (2')$$

where H_V is the Vickers Hardness of the material in (kg$_f$/mm^2) (equal to 175 kg$_f$/mm^2 for AA7075-T6 [22]) and $\sqrt{\text{area}}$ (in (μm)) is the square root of the area of the defect projected onto a plane perpendicular to the load axis.

Considering, for example, the crack initiation regions shown in Figs. 5 and 6, $\sqrt{\text{area}}$ was equal to 70 μm and 60 μm, respectively. In very high cycle fatigue of steels, fatigue crack initiation can be assessed by ODA or the "fish-eye." Here, the former value was assumed and determined considering the total area of the observed ODA (Fig. 5c). Considering, instead, the subsurface failure (Fig. 6c) where no ODA was revealed, the calculated value corresponds to the ellipse circumscribed to the small material region characterised by a different chemical composition with respect to the surrounding one. By applying Eqs. (2) and (2′), the obtained $\sqrt{\text{area}}$ values allowed for the determination of the corresponding endurance strengths at 5x10^9 cycles, equal to σ_w = 113 MPa and σ_w = 105 MPa, respectively. Such values seem to be comparable to the service stresses determined by the FEM analysis for both the rectangular and the circular sonotrodes. Generalizing the appli-

cation of the method to the initiation regions of each fracture surface of the two sonotrodes, the lowest endurance limit at 5×10^9 cycles resulted to be equal to 93 MPa, thus, helping to clarify the reason of the premature failures.

5. Concluding remarks

The premature failures of two sonotrodes made from AA7075-T6 and used for the ultrasonic welding of thermoplastics were analysed. The results can be summarised as follows:

- application of the liquid penetrants NDT method allowed for the understanding that the failures were due to the premature (after 5×10^9 cycles when 10^{12} were expected) initiation of fatigue cracks at stress concentrations;
- SEM observations of the fracture surfaces showed two distinct crack initiation modes: the presence of "optically dark areas" in the interior of the material and of metallurgical defects at the subsurface close to geometrical stress concentrations;
- metallurgical analyses demonstrated that the chemical composition of the aluminium alloy was correct, but with extremely high segregation at grain boundaries;
- segregation was found to be the cause for both of the crack initiation modes;
- considering the "optically dark areas" and contrary to what usually occurs in steels, endogenous defects (the segregation) and the oxygen trapped inside them seemed to play a fundamental role;
- careful and innovative, at least for the ultrasonic welding field, dynamical FEM analyses made it possible to derive the service stress levels at initiation regions;
- the relationship between the dimension of initiation defects and the fatigue endurance strength was defined in terms of Murakami's theory, allowing for a comparison with the service stresses and the understanding of the premature failures.

Acknowledgements

The author would like to thank Dr. Massimiliano Annoni and Mr. Mario Ferraris for their support and helpful discussions. Moreover, special thanks goes to Mr. Bruno Minniti for his help with the finite element analyses and to Dr. Silvia Barella for her help with the metallurgical analyses.

References

[1] German Electrical Manufacturers Association (ZVEI), Ultrasonic assembly of thermoplastic moldings and semi-finished products, Frankfurt; 1980.
[2] Annoni M, Carboni M. Ultrasonic metal welding of AA 6022-T4 lap joints: Part I – Technological characterisation and static mechanical behaviour. Sci Technol Weld Joi 2011;16:107–15.
[3] Carboni M, Annoni M. Ultrasonic metal welding of AA 6022-T4 lap joints: Part II – Fatigue behaviour, failure analysis and modelling. Sci Technol Weld Joi 2011;16:116–25.
[4] Plastics Design Library, Handbook of plastics joining: a practical guide, New York; 1997.
[5] Grewell DA, Benatar A, Park JB, editors. Plastics and composites welding handbook, Cincinnati; 2003.
[6] Bathias C, Paris PC. Gigacycle fatigue in mechanical practice, New York; 2005.
[7] Goldstein GI, Newbury DE, Echlin P, Joy DC, Fiori C, Lifshin E. Scanning electron microscopy and X-ray microanalysis, New York; 1981.
[8] Bathias C. There is no infinite fatigue life in metallic materials. Fatigue Fract Eng Mater Struct 1999;22:559–65.
[9] Miller KJ, O'Donnell WJ. The fatigue limit and its elimination. Fatigue Fract Eng Mater Struct 1999;22:545–57.
[10] Wang QY, Li T, Zeng XG. Gigacycle fatigue behaviour of high strength aluminium alloys. Proc Eng 2010;2:65–70.
[11] Hull D. Fractography: Observing. Cambridge: Measuring and Interpreting Fracture Surface Topography; 1999.
[12] Murakami Y, Yokoyama NN, Nagata J. Mechanism of fatigue failure in ultralong life regime. Fatigue Fract Eng Mater Struct 2002;25:735–46.
[13] ASTM. Annual book of ASTM standards – section 2: nonferrous metal products, vol. 02.02. Aluminium and Magnesium Alloys, Philadelphia; 1996.
[14] ASM international, materials characterisation. ASM Handbook, vol. 10. Cleveland; 1986.
[15] Amin SG, Ahmed HMM, Youssef HA. Computer-aided design of acoustic horns for ultrasonic machining using finite-element analysis. J Mater Proc Technol 1995;55:254–60.
[16] Nad M, Cicmancova L. The effect of the shape parameter on modal properties of ultrasonic horn design for ultrasonic assisted machining. Proc. 8th international DAAAM Baltic conference, Tallinn, Estonia; 2012.
[17] ABAQUS, vol. 6.10-1. User's manual; 2011 <http://www.3ds.com/>.
[18] Minniti B. Analysis of the dynamic behaviour of an ultrasonic welder for plastic materials. MSc thesis. Milano; 2012.
[19] Mayer H, Papakyriacou M, Pippan R, Stanzl-Tschegg S. Influence of loading frequency on the high cycle fatigue properties of AlZnMgCu1.5 aluminium alloy. Mater Sci Eng A 2001;314:48–54.
[20] Wang QY, Kawagoishi N, Chen Q. Fatigue and fracture behaviour of structural Al-alloys up to very long life regimes. Int J Fatigue 2006;28:1572–6.
[21] Murakami Y. Metal fatigue: effects of small defects and non-metallic inclusions, Oxford; 2002.
[22] http://www.matweb.com/index.aspx.